ACS OMEGA

Open Access

http://pubs.acs.org/journal/acsodf

Article

Gold Nanoparticle−mRNA Conjugates Encapsulated in Lipid Nanoparticles for Coordinated Codelivery of Multiple mRNAs

Dajeong Hwang,[#] Sin A Park,[#] Jae Hoon Kim, Seung-Yeul Lee, Jaebeom Lee, Han Sang Kim, Kyung-A Kim, Seung-Hoon Lee, Tae Jeong Oh, Jaewook Lee,* and Sungwhan An*

Cite This: *ACS Omega* 2025, 10, 32998−33007

Read Online

ACCESS | Metrics & More | Article Recommendations | Supporting Information

ABSTRACT: Gold nanoparticles (AuNPs) can be engineered to be utilized as carriers via anchoring multiple nucleic acids, including mRNAs, in specific ratios. However, the negative charge of mRNA−AuNP conjugates presents significant challenges for efficient cellular uptake and subsequent expression. To overcome this limitation, we developed a delivery system that combines mRNA−AuNP conjugation with lipid nanoparticles (LNPs) to enhance intracellular delivery. In our approach, AuNPs were functionalized with a thiolated antisense leader sequence (ALS), oligonucleotides complementary to the 5′-end leader sequence of the 5′-untranslated region (UTR) of the mRNA. This functionalization resulted in the formation of mRNA−ALS−AuNP conjugates, which were then encapsulated within LNPs. When we compared the ALS-AuNP@LNP constructs to ALS−AuNPs alone, ALS-AuNP@LNP demonstrated superior delivery and expression of *enhanced green fluorescence protein* (*EGFP*) mRNA across multiple cell lines, as evidenced by robust green fluorescence. Furthermore, this system enables the precise codelivery of multiple mRNAs in defined ratios, as demonstrated by the successful codelivery of *EGFP* and *mCherry* mRNAs. These findings highlight the potential of the mRNA-ALS-AuNP@LNP platform as an effective and versatile tool for advancing mRNA-based therapeutics and vaccine development.

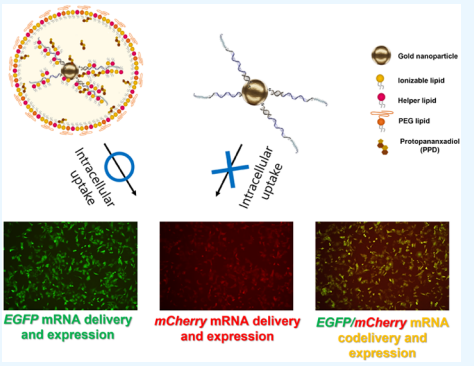

INTRODUCTION

In the postpandemic era, the development of nucleic acid-based therapeutics and vaccines has accelerated significantly, with mRNA platforms emerging as a transformative technology due to their rapid design capabilities, high efficacy, and broad accessibility.[1−3] These attributes have driven a surge in preclinical and clinical trials for mRNA-based vaccines and gene therapies worldwide.[4−8] Despite these advances, achieving efficient and stable delivery of mRNA remains a major challenge in clinical applications, highlighting the critical need for optimized delivery systems.

Various carriers for mRNA delivery have been explored, including viral vectors, exosomes, polymeric nanoparticles, inorganic nanoparticles, and lipid nanoparticles (LNPs).[9−14] Among these, gold nanoparticles (AuNPs) have garnered particular interest because of their excellent biocompatibility, low toxicity, and ease of functionalization through thiol chemistry.[15−18] This functionalization allows for the attachment of mRNAs, enabling precise codelivery of nucleic acids in controlled ratios.[19−24] Especially, the capture probes on AuNP surfaces can facilitate the controlled loading of not only two types of nucleic acids (e.g., mRNA and siRNA) but also triple or more different nucleic acid types under well-regulated conditions.[25,26] It means AuNPs can play a role as a scaffold for multiple mRNA delivery platforms. Additionally, the unique plasmonic and electromagnetic properties of AuNPs enhance their suitability for theranostic applications, such as hyperthermia, imaging agents, and CT contrast agents.[27−30] In addition, anchored nucleic acid on the AuNPs was protected against nuclease, so AuNPs were considered as a suitable carrier for a gene delivery system.[31,32] These features support their potential in multimodal therapeutic strategies aimed at addressing unmet medical needs.[33−35]

However, the intrinsic negative charge of mRNA−AuNP conjugates presents a significant barrier to cellular uptake due to electrostatic repulsion. On the other hand, LNPs have proven to be an effective solution to this limitation and have established themselves as reliable carriers for mRNA delivery, as evidenced by their crucial role in the success of mRNA vaccines.[36−39]

In this study, we harnessed the complementary strengths of AuNPs and LNPs by developing an LNP-encapsulated gold nanoparticle (AuNP@LNP) system for mRNA delivery. Briefly, AuNPs were modified with antisense leader sequences (ALS), which are thiolated oligonucleotides complementary to

Received: March 7, 2025
Revised: June 25, 2025
Accepted: July 15, 2025
Published: July 25, 2025

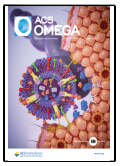

Table 1. ALS and Leader Sequence (5′UTR) Used in This Study

oligomers	sequences (5′ to 3′)
ALS 30mer	*GGAAGGTATAAACCTTTAATAAAAAAAAAA[Thiol]*
ALS 50mer	*GTTGGTTGGTTTGTTACCTGGGAAGGTATAAACCTTTAATAAAAAAAAAA[Thiol]*
leader	*ATTAAAGGTTTATACCTTCCCAGGTAACAAACCAACCAACTTTCGATCTCTTGTAGATCTGTTCTCTAAACGAACAAACTAAA*

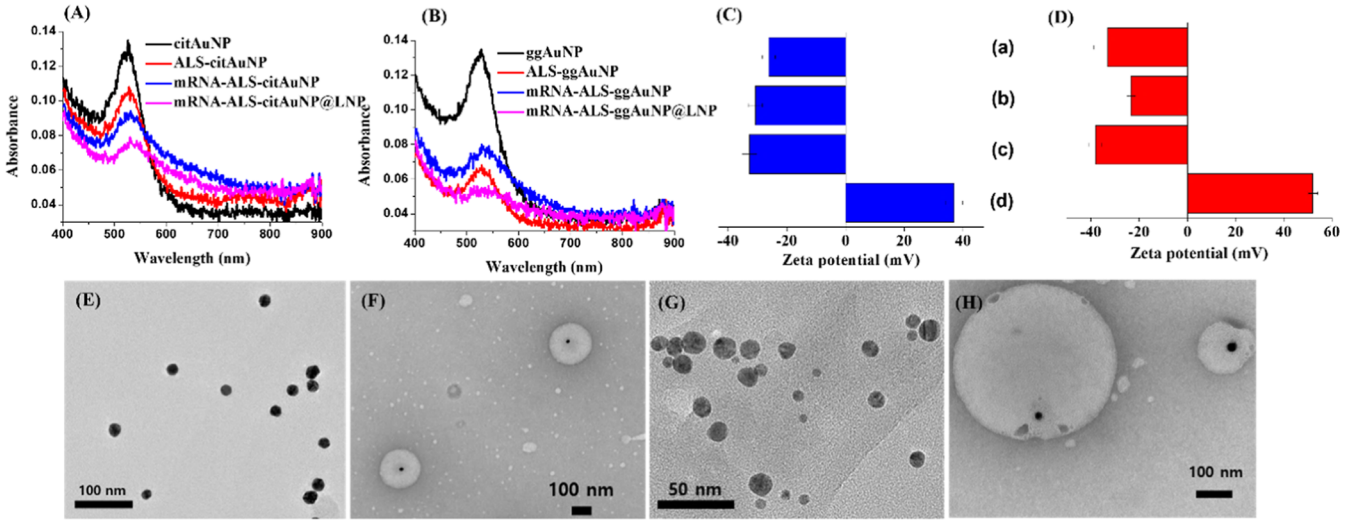

Figure 1. Physicochemical characterization of (A) and (C) citAuNP and (B) and (D) ggAuNP depending on the surface modification with mRNA and LNP; (A) and (B) UV/vis spectra for measurement of plasmonic absorbance, (C) and (D) zeta potential shift ((a) AuNPs, (b) ALS−AuNPs, (c) *EGFP* mRNA−ALS−AuNPs, and (d) *EGFP* mRNA-ALS-AuNP@LNP), and TEM images of (E) cit-AuNP, (F) *EGFP* mRNA-ALS-citAuNP@LNP, (G) ggAuNP, and (H) *EGFP* mRNA-ALS-ggAuNP@LNP.

the 5′ untranslated region (UTR) of mRNA, leading to the assembly of the mRNA−ALS−AuNP structure. The ALS and 5′-end leader sequence (5′UTR of mRNA) used in this study are detailed in Table 1. And two types of AuNPs were employed in this study: citrate-coated AuNPs (citAuNPs) and gelatin-gallic acid-coated AuNPs (ggAuNPs). To further enhance cellular uptake, the mRNA−ALS−AuNP complexes were encapsulated with protopanaxadiol (PPD)-based lipid nanoparticles (LNPs), which were previously developed by our group.[36] Our findings demonstrated that LNP-encapsulated mRNA−ALS−AuNPs showed significant enhancement of cellular uptake and protein expression, significantly. Moreover, this system enabled the codelivery of multiple mRNAs, as illustrated by the simultaneous delivery of *EGFP* and *mCherry* mRNAs. These results highlight the potential of the mRNA-ALS-AuNP@LNP platform as a versatile and effective approach to advancing mRNA-based therapeutics and vaccines.

RESULTS AND DISCUSSION

Characterization of AuNPs and mRNA-ALS-AuNP@LNP. To advance AuNP-based mRNA delivery systems, we initially synthesized two types of AuNPs: citAuNP and ggAuNP. The physicochemical properties of these AuNPs were analyzed to evaluate their suitability for mRNA delivery. First, the functional groups of each AuNP were analyzed using Fourier transform infrared (FT-IR) spectroscopy, as shown in Figure S1A. The vibration band at 1570 cm^{-1} in both AuNPs indicated the antisymmetric stretching mode of COO^- groups from citrate, gelatin, and gallic acid on the AuNP. The vibration mode of the amide bond in gelatin showed around 1765 cm^{-1}, and the band around 1470 cm^{-1} was characteristic of benzene from gallic acid. Second, the plasmonic property of both AuNPs was characterized and is shown in Figure 1A,B. In this case, the plasmonic band of citAuNP and ggAuNP was observed around 520 nm and the absorbance spectrum of both AuNPs was not shifted after surface modification with ALS, mRNA, and LNP encapsulation. This indicates that the stability of AuNPs was maintained, and no particle aggregation occurred during surface modification with mRNA and the encapsulation process. Consequently, the change of zeta potential of both AuNPs was monitored after surface modification and encapsulation (Figure 1C,D). In this case, AuNP, ALS−AuNP, and mRNA−ALS−AuNP structures exhibited a clear negative charge ((a), (b), and (c)). However, the surface charge was shifted from negative to positive potential after the LNP encapsulation process (d). This positive charge in the *EGFP* mRNA-ALS-AuNP@LNP plays a crucial role in charge-dependent cellular uptake. It is well established that positively charged delivery systems demonstrate enhanced cellular penetration.[40−42]

The surface modification of AuNPs with ALS and mRNA was further analyzed using gel electrophoresis, Qubit assay, and RiboGreen assay. According to the electrophoresis results in Figure S1B, the position of ALS-citAuNP and ALS-ggAuNP was clearly migrated. After mRNA hybridization, both ALS−AuNPs exhibited a shift in position, indicating a successful surface modification. The binding efficiency of ALS to AuNP was evaluated and optimized depending on the various amounts of ALS ranging from 10 pmol to 30 pmol through a Qubit assay and eq 1 in the Methods part, revealing that approximately 77% of ALS attached to citAuNP at 15 pmol (Figure S1C). Based on this result, the same concentration (15 pmol) of ALS was used for surface modification of ggAuNP to capture the mRNA. Furthermore, the hybridization efficiency of *EGFP* mRNA with ALS on the AuNP surface was evaluated

https://doi.org/10.1021/acsomega.5c02145
ACS Omega 2025, 10, 32998−33007

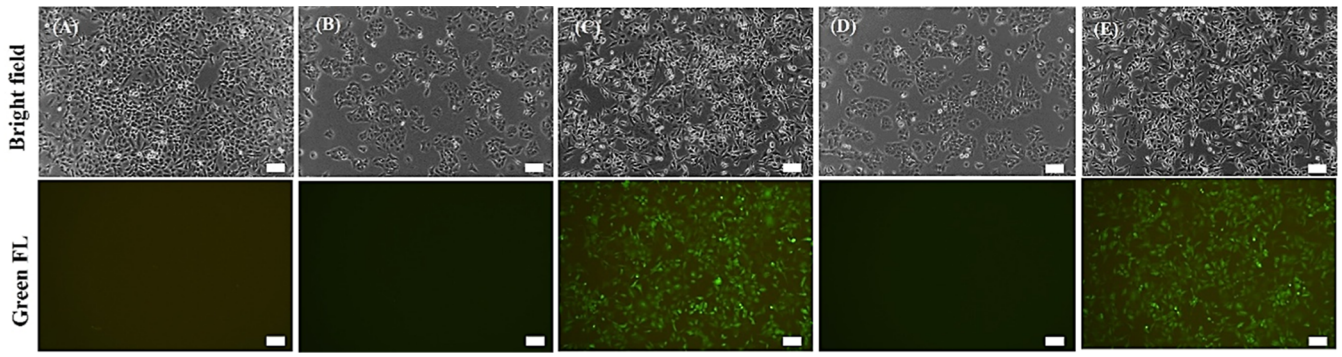

Figure 2. Monitoring of EGFP expression in A549 cells depending on the LNP encapsulation process. (A) Nontreated, (B) *EGFP* mRNA-ALS-citAuNP, (C) *EGFP* mRNA-ALS-citAuNP@LNP, (D) *EGFP* mRNA-ALS-ggAuNP, and (E) *EGFP* mRNA-ALS-ggAuNP@LNP (scale bar: 100 μm).

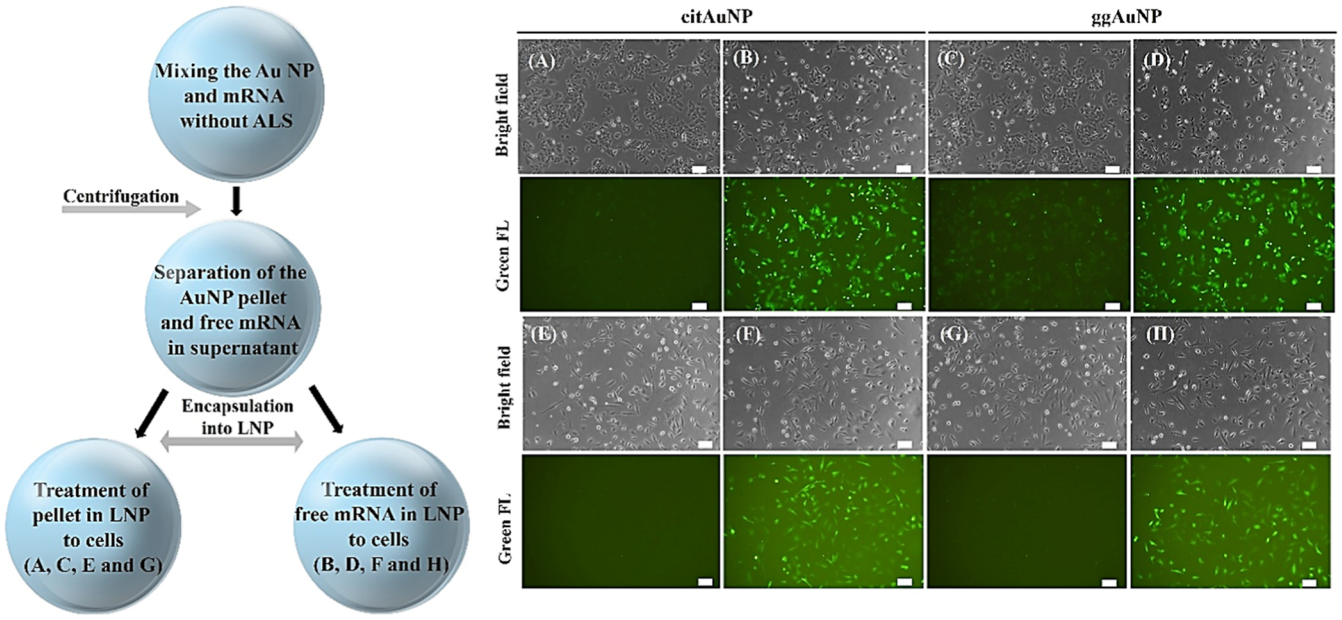

Figure 3. Schematic diagram of the experiment (left) and observation of EGFP expression without ALS in the AuNP@LNP platform in A549 (A to D) and HeLa cells (E to H). (A, E) Pellet citNP@LNP and (B, F) free *EGFP* mRNA@LNP in citAuNP conditions, (C, G) pellet ggAuNP@LNP, and (D, H) free *EGFP* mRNA@LNP in ggAuNP conditions (scale bar: 100 μm).

using a RiboGreen assay and eq 2 in the Methods part, showing that approximately 20% and 19% of the mRNA was bound to ALS on citAuNP and ggAuNP, respectively. These results aligned with the gel electrophoresis results that exhibited residual bands corresponding to unbound mRNA in (h) and (i) of the right image in Figure S1B. Although these values were slightly lower than anticipated, future optimization will be conducted for an in vivo test to enhance the delivery and expression performance and mRNA-based therapeutic outcomes. The encapsulation efficiency of AuNPs within LNP was assessed using the electrophoresis results shown in Figure S1B. If the mRNA−ALS−AuNP complex had not been effectively encapsulated, a residual red band—similar to the one seen in lane (h)—would have appeared in lane (j). However, the absence of such a residual band in lane (j) meant that almost all the mRNA−ALS−AuNP complex was successfully encapsulated within the LNP. The stability of mRNA on the AuNP was evaluated against RNase. If the mRNA on the AuNP was degraded or damaged by RNase, the AuNP band would have either shifted significantly similar to that observed in (h) and (f) of Figure S1B or reverted to a position resembling (a) in Figure S2. However, gel electrophoresis results in Figure S2 showed no notable shift in the *EGFP* mRNA-ALS-citAuNP band after RNase treatment, indicating that the mRNA remained intact on the AuNP and was effectively protected from RNase degradation. On the other hand, *EGFP* mRNA was fully degraded by RNase without AuNPs (lane (c) in Figure S2).

The morphology and structure of AuNPs and *EGFP* mRNA-ALS-AuNP@LNP were observed using FE-TEM and bio-TEM (Figure 1E−H). The results revealed that both types of AuNPs possessed a polygonal shape and were well dispersed without aggregation ((E) and (G)). Also, the AuNP-encapsulated LNPs were exhibited ((F) and (H)). The particle size variations at each modification step were evaluated using the nanoparticle tracking analysis (NTA) system (Figure S1D,E). The sizes of AuNPs, ALS−AuNPs, and mRNA−ALS−AuNPs showed no significant differences, which correlated well with their respective plasmonic absorption spectra, which were not shifted following surface modification. However, after encapsulation with LNPs, the particle sizes increased noticeably, with *EGFP* mRNA-ALS-citAuNP@LNP and *EGFP*

https://doi.org/10.1021/acsomega.5c02145
ACS Omega 2025, 10, 32998−33007

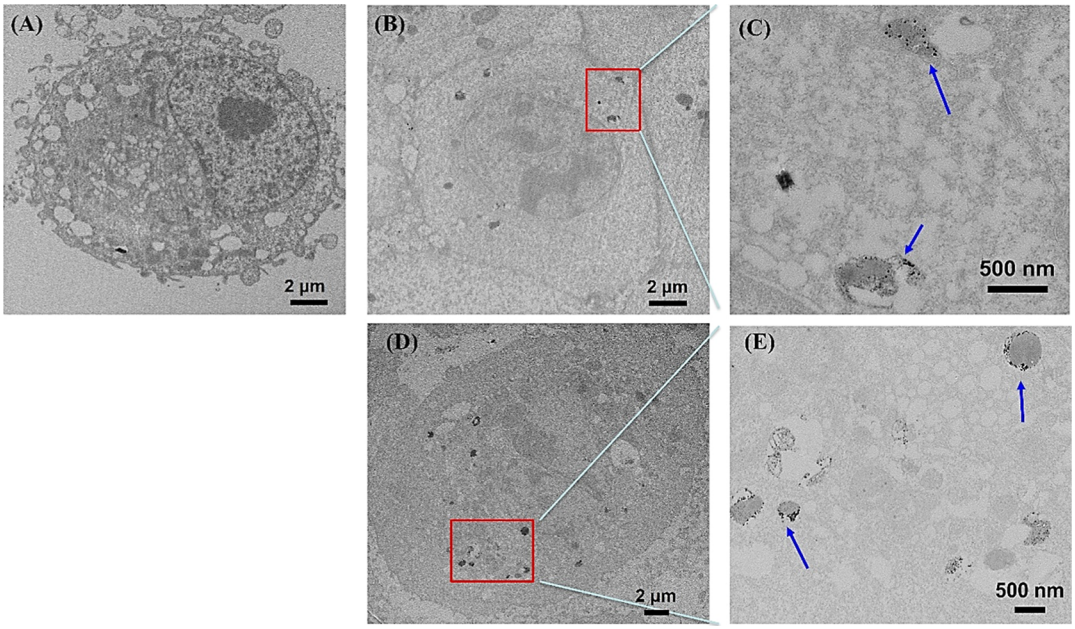

Figure 4. TEM images of A549 cells; (A) nontreated condition, (B) and (C) *EGFP* mRNA-ALS-citAuNP@LNP-treated A549 cell, (D) and (E) *EGFP* mRNA-ALS-ggAuNP@LNP-treated A549 cell. Blue arrows in (C) and (E) indicate AuNPs.

mRNA-ALS-ggAuNP@LNP measuring approximately 131.4 and 129.3 nm, respectively. These sizes are within the optimal range for cellular uptake. Furthermore, biocompatibility tests in A549 cells were performed under various concentrations, and they showed minimal cytotoxicity (∼10%) even at high concentrations (Figure S3). Furthermore, our previous study confirmed the biocompatibility of PPD-containing LNPs,[36] suggesting that AuNP-LNP systems also possessed biocompatible properties.

mRNA Delivery and Expression by Using the ALS-AuNP@LNP Vehicle. The delivery efficacy and expression efficiency of the AuNP@LNP system were evaluated using *EGFP* mRNA in the A549 cell line. After treatment of *EGFP* mRNA-ALS-AuNP without an LNP shell, EGFP expression was not detected in A549 cells (Figure 2B and D). However, green fluorescence indicative of EGFP expression was clearly observed in cells treated with *EGFP* mRNA-ALS-citAuNP@LNP or *EGFP* mRNA-ALS-ggAuNP@LNP (Figure 2C and E). This observation is consistent with the zeta potential results, highlighting charge interactions as a critical factor in the cellular uptake. Cells exhibited a negative surface charge due to their lipid bilayer,[43,44] and *EGFP* mRNA−ALS−AuNPs also showed a negative charge. This charge similarity could lead to repulsion, potentially hindering cellular uptake.[45−48] In contrast, positively charged *EGFP* mRNA-ALS-AuNP@LNP could be taken up by the cells through charge interactions, enabling effective mRNA delivery and subsequent expression. Additionally, EGFP expression in DAPI-stained A549 cells was visualized by using confocal microscopy, as shown in Figure S4. In the image, the green fluorescence from EGFP corresponds to the cellular structure and overlaps with the DAPI-stained nuclei, indicating successful intracellular expression.

Conversely, we hypothesized that AuNPs without ALS would be unable to capture mRNA, preventing them from delivering mRNA into cells and hindering its expression. To validate this, we investigated *EGFP* mRNA delivery and expression under conditions where AuNPs lacked ALS. As illustrated on the left in Figure 3, *EGFP* mRNA was mixed with citAuNP or ggAuNP, followed by centrifugation to separate unbound free mRNA from the AuNP pellet. Both the free mRNA and the AuNP pellet were then encapsulated with LNP and treated with A549 and HeLa cells to assess the EGFP expression. The expression results showed that green FL was primarily observed in the supernatant containing unbound *EGFP* mRNA in both A549 and HeLa cells (Figure 3B, D, F, and H). For ggAuNPs without ALS, a slight green FL was detected, likely due to nonspecific binding of *EGFP* mRNA to the particles (Figure 3C). According to the literature, gelatin-based nanoparticles can capture nucleic acids through charge interactions and their polymeric matrix, which likely explains the nonspecific binding observed with ggAuNPs in this study.[49−52] However, the green FL images in cells clearly indicate that the mRNA delivery and expression efficiency of this system were significantly lower compared to those of the ALS-AuNP@LNP carrier.

Optimization of mRNA Delivery and Expression. The effect of ALS length on mRNA delivery and expression was analyzed considering its role in ribosome binding for translation. Our hypothesis suggested that if the ribosome binding site in the 5′ UTR leader sequence of the mRNA was insufficient after ALS hybridization, translation efficiency could be reduced to produce the protein. To test this, EGFP expression was compared between ALS lengths of 50 mer and 30 mer after *EGFP* mRNA delivery. In both AuNP@LNP carriers, cells exhibited stronger green fluorescence under the ALS 30 mer condition than under the ALS 50 mer condition (Figure S5). These findings confirm that ALS length plays a crucial role in protein production.

The weight ratio between mRNA and LNP (w: w) is one of the key factors for effective delivery and expression. In this study, the weight ratio was varied to optimize mRNA delivery and expression, with experiments conducted in the HEK293T cell line (Figure S6). The optimal mRNA-to-LNP weight ratio was identified as 1:5, with comparable efficiency observed at ratios of 1:2 and 1:10. These results highlighted the mRNA-to-

https://doi.org/10.1021/acsomega.5c02145
ACS Omega 2025, 10, 32998−33007

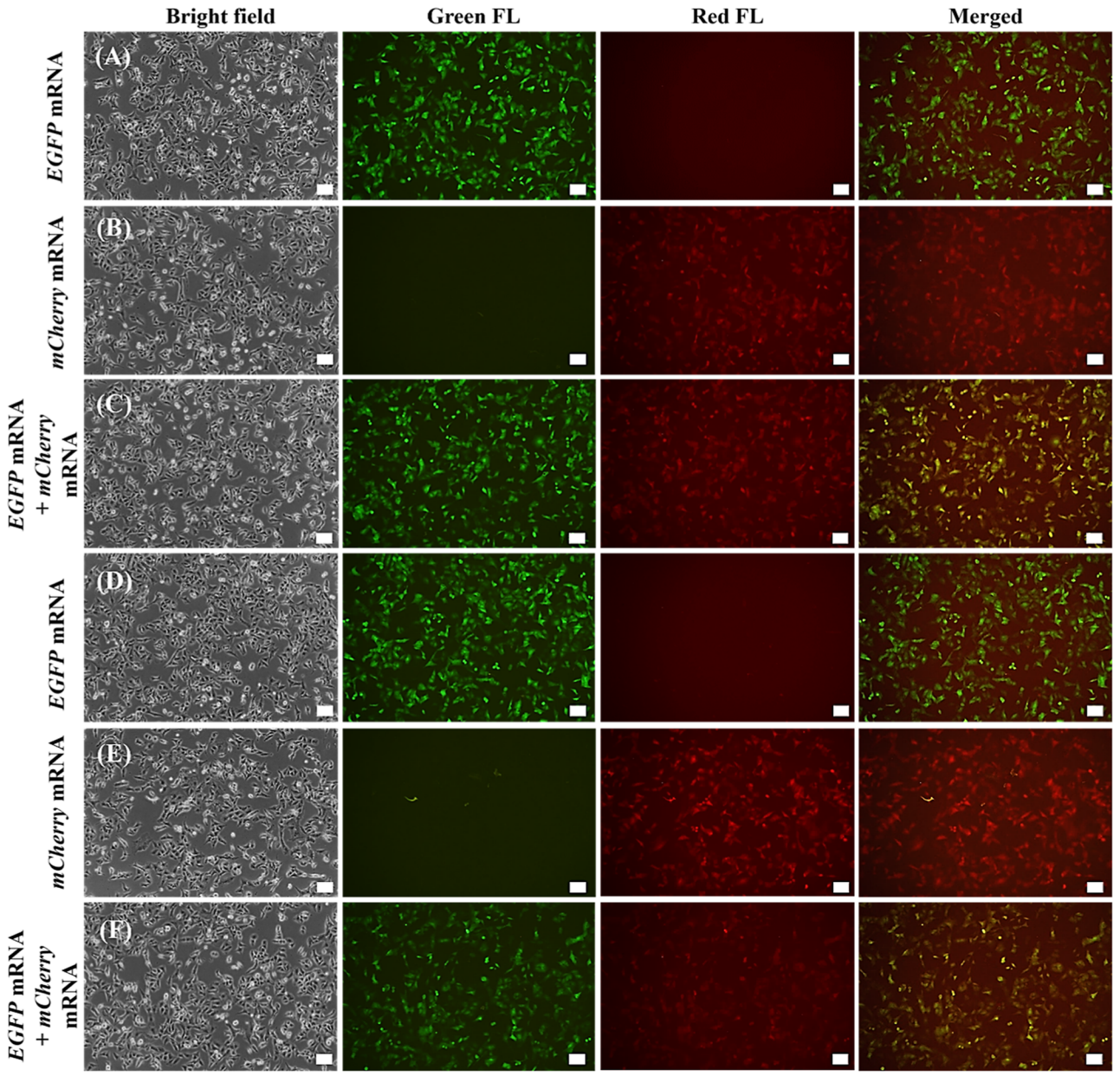

Figure 5. *EGFP*/*mCherry* mRNA codelivery and expression test. (A) *EGFP* mRNA, (B) *mCherry* mRNA, and (C) *EGFP*/*mCherry* mRNA delivery by using ALS-citAuNP@LNP and (D) *EGFP* mRNA, (E) *mCherry* mRNA, and (F) *EGFP*/*mCherry* mRNA delivery by using ALS-ggAuNP@LNP (scale bar: 100 μm).

LNP weight ratio as a key factor for efficient mRNA delivery and expression.

Cellular Uptake. The cellular uptake of mRNA-ALS-AuNP@LNPs was observed by using bio-TEM (Figure 4). Nanoparticle (NP) uptake mechanisms are highly complex and typically include nonspecific endocytosis, charge interactions, phagocytosis, pinocytosis, and receptor-mediated endocytosis (RME).[48,53−59] In this study, positively charged mRNA-ALS-AuNP@LNP was able to penetrate into the cell through a charge interaction-based endocytosis process. Moreover, the AuNPs did not aggregate or form large particles within the cytoplasm (as indicated by blue arrows in the images). This stability indicates that the attached *EGFP* mRNA remained intact within the cell, avoiding damage from particle aggregation, thereby enabling successful EGFP expression.

Furthermore, the targeted delivery capability of mRNA-ALS-AuNP@LNP was assessed following the folate modification of the LNP surface. *EGFP* mRNA-ALS-citAuNP@folate-LNP or *EGFP* mRNA-ALS-ggAuNP@folate-LNP could bind with folate receptors (FR) in HeLa cells, which highly express the FR; the green fluorescence of EGFP was more intense compared with the *EGFP* mRNA-ALS-AuNP@LNP condition ((A) to (E) in Figure S7). In contrast, the opposite trend was observed in the FR-negative A549 lung cancer cell line (F-J in Figure S7), confirming the receptor-specific targeting effect.

Co-mRNA Delivery and Expression Using the ALS-AuNP@LNP Vehicle. The platform's potential for dual mRNA delivery was demonstrated using *mCherry* and *EGFP* mRNAs. Fluorescence imaging and flow cytometry confirmed tunable expression of both mRNAs in A549 cells, with expression levels modulated by their mixing ratios, showcasing

https://doi.org/10.1021/acsomega.5c02145
ACS Omega 2025, 10, 32998−33007

the platform's flexibility for complex therapeutic applications. Furthermore, our hypothesis suggested that the ALS-AuNP delivery system could carry not only a single mRNA structure but also two different mRNA structures simultaneously. To test this concept, *mCherry* mRNA and *EGFP* mRNA were hybridized with ALS on citAuNP or ggAuNP at various mixing ratios, and after encapsulation with LNP, A549 cells were treated with these structures (Figure 5). After treatment, the green FL and red FL were clearly observed in the A549 cells, with the merged images showing an orange color. It indicated that both mRNAs were successfully delivered and their respective fluorescent proteins were expressed. Also, the FL images demonstrated that as the proportion of *mCherry* mRNA increased and *EGFP* mRNA decreased in the structure, the brightness of red and green FL in the cells was tuned accordingly. These results validated the capability of this system to regulate protein expression by adjusting the delivery of both mRNAs. Flow cytometry analysis further supported this, showing that the mean fluorescence intensity (MFI) shifted under the ratio between the two types of mRNA (Figure S8). These results indicate that it is possible for our platform to deliver multiple mRNAs into a cell with a precisely controlled stoichiometric ratio. Indeed, for successful antibody production, both heavy-chain and light-chain mRNAs must be delivered under precisely controlled conditions, and their corresponding proteins must be efficiently expressed. This highlights the critical importance of dual mRNA delivery and expression in antibody development. As such, the ALS-AuNP@LNP system offers the versatility and potential required for efficient antibody synthesis and other complex therapeutic applications.

CONCLUSION

In this study, we aimed to address the challenge of delivering negatively charged gene carriers under precise control into cells for efficient protein expression by introducing an LNP-encapsulated mRNA−ALS−AuNP system. To validate this approach, two types of AuNPs, citAuNP and ggAuNP, were functionalized with thiolated ALS on their surface to capture *EGFP* mRNA. And these complexes were then encapsulated within the LNP. Importantly, the plasmonic properties of the AuNPs remained unchanged after mRNA loading and LNP encapsulation, indicating no aggregation occurred during the process. Furthermore, LNP encapsulation helped protect the mRNA on the AuNP from RNase degradation and enabled targeted delivery to specific cell lines through surface modification. The delivery efficiency and protein expression were then assessed across various cell lines. As expected, EGFP expression was observed in the case of positively charged *EGFP* mRNA-ALS-AuNP@LNP in several cell lines. Furthermore, successful codelivery and expression of *EGFP* and *mCherry* mRNAs confirmed that the mRNA remained intact and functional throughout delivery. Because the thiolated ALS on the AuNP can specifically bind to both *EGFP* and *mCherry* mRNAs, it enables controlled codelivery and expression of the two mRNA types. These findings highlight the potential of the ALS-AuNP@LNP hybrid system for multiple mRNA delivery platforms and multimodal therapeutic applications. Future research will focus on extending the application of these AuNP and LNP-based gene delivery systems to gene therapy, including in vivo testing.

MATERIALS AND METHODS

Materials and Instruments. $HAuCl_4{\cdot}3H_2O$, trisodium citrate, sodium borohydride, gallic acid, and gelatin type B were purchased from Sigma-Aldrich (Yongin, Republic of Korea). Protopanaxadiol (PPD), 1,2-dioleoyl-*sn*-glycero-3-phosphoethanolamine (DOPE, phospholipid), heptadecan-9-yl 8-[2-hydroxyethyl-(6-oxo-6-(undecyloxy) hexyl) amino] octanoate (SM-102, ionizable lipid), and 1,2-dimyristoyl-rac-glycero-3-methoxypolyethylene glycol-2000 (DMG 2000, PEG lipid) were bought from Cayman Chemical (Ann Arbor, MI, USA). 1,2-Distearoyl-*sn*-glycero-3-phosphoethanolamine-N-folate [(polyethylene glycol)-2000] (DSPE-PEG(2000)-folate) was purchased from BroadPharm (San Diego, CA, USA). The thiolated antisense leader sequence (ALS) for hybridization with the leader sequence in the 5′UTR of mRNA was purchased from Bioneer (Daejeon, Republic of Korea). Dulbecco's Modified Eagle Medium (DMEM), Fetal Bovine Serum (FBS), phosphate buffered saline (PBS), Penicillin−Streptomycin, and RPMI were purchased from Welgene (Gyeongsan, Gyeongsangbuk-do, South Korea), and 96-, 24-, and 6-well plates were bought from Thermo Fisher Scientific (Waltham, MA, USA) for cell culture. A549, HeLa, and HEK293T cells were obtained from the Korean Cell Line Bank (Seoul, Republic of Korea). The Qubit assay for analysis of thiolated ALS modification on AuNP and the Quant-iT RiboGreen RNA assay kit for mRNA conjugation were bought from Invitrogen/Thermo Fisher Scientific (Seoul, Republic of Korea). The cell counting kit-8 (CCK-8) assay kit was purchased from Dojindo (Kumamoto, Kyushu, Japan). For nuclear DAPI staining, Vectashield HardSet mounting medium was obtained from Vector Laboratories (CA, USA).

The morphology of AuNPs and mRNA-ALS-AuNP@LNP was observed by using field emission transmission electron microscopy (FE-TEM, JEM-F200, JEOL, Tokyo, Japan) and bio-TEM (H-7600, Hitachi, Tokyo, Japan), respectively. The size of the mRNA-ALS-AuNP@LNP was measured through nanoparticle tracking analysis (NTA, NanoSight NS300, Malvern Panalytical, Malvern, UK), and the surface zeta potential of AuNP and mRNA-ALS-AuNP@LNP was characterized through Zeta sizer (Nano ZS, Malvern Panalytical, Malvern, UK). The plasmonic absorbance of AuNPs as well as the CCK-8 assay for cell viability was measured by using a microplate spectrophotometer (Mobi, MicroDigital, Seongnam, Republic of Korea). The fluorescence (FL) intensity was monitored by a microplate multimode reader (BioTek Synergy HTX, Agilent, Santa Clara, CA, USA). The mRNA quantification was performed using a microvolume spectrophotometer (NanoDrop, Thermo Fisher Scientific, Waltham, MA, USA). The EGFP and mCherry-positive cells and mean of FL intensity (MFI) were analyzed via flow cytometry (BD FACSLyric, BD Bioscience, Franklin Lakes, NJ, USA). The cell morphology and expression of EGFP and mCherry in the cells were observed using a fluorescent optical microscope (CKX553, Olympus, Tokyo, Japan). Also, the expression of EGFP in DAPI-stained A549 was observed via confocal microscopy (LSM 710, Carl Zeiss, Oberkochen, Germany).

METHODS

Synthesis of citAuNP and ggAuNP. citAuNP was synthesized using $HAuCl_4{\cdot}3H_2O$ and trisodium citrate. Initially, 7.6 μmol of $HAuCl_4{\cdot}3H_2O$ was dissolved in 40 mL

https://doi.org/10.1021/acsomega.5c02145
ACS Omega 2025, 10, 32998−33007

of D.I. water, and then this solution was heated at 130 °C for 20 min. Subsequently, 27 μmol of sodium citrate in 3 mL of D.I. water was added to the Au salt solution, which was then stirred and maintained at 130 °C for 2 h. After reaction, the reddish citAuNP solution was cooled to R.T. (room temperature) and purified by centrifugation at 1000 rpm for 10 min to remove aggregates. Next, for the synthesis of the ggAuNP, 12.7 μmol of $HAuCl_4 \cdot 3H_2O$ was dissolved in 30 mL of PBS. Subsequently, 1 mL of 1 wt % gelatin (type B) was added, and the mixture was heated at 120 °C for 1 min. After that, 0.3 mL of a 0.01 M gallic acid solution was dropped into the mixture, and this solution was heated and stirred at 120 °C for 2 h. The ggAuNP solution was then cooled to R.T., and it was purified via centrifugation at 10,000 rpm for 10 min.

Preparation of mRNA-ALS-AuNP@LNP. The mRNA-ALS-AuNP@LNP complex was synthesized in three steps, which were surface modification of citAuNP or ggAuNP with ALS, hybridization of mRNA with ALS−AuNP, and encapsulation of mRNA−ALS−AuNP into LNP. The detailed experimental procedure was as follows.

First, to attach the ALS on both AuNPs, 15 pmol of ALS and 10 μg of each AuNP were mixed in 10 μL of acidic citrate buffer, which was composed of 500 mM trisodium citrate solution and HCl to facilitate fast and spontaneous modification of ALS on the AuNPs in 30 min at R.T. without a long-term salting aging process.[60] After the modification reaction, unbound ALS was isolated and eliminated by centrifugation at 10,000 rpm, 20 min. The efficiency of ALS modification on the AuNP was estimated by using a Qubit assay kit by measuring FL intensity at an excitation wavelength of 500 nm and an emission wavelength of 525 nm with a Qubit Fluorometer.

Second, the hybridization step between mRNA and ALS on AuNP was performed as follows. The ALS-citAuNP or ALS-ggAuNP from the first step was dispersed in 40 μL of hybridization buffer, which was composed of 30 mM HEPES buffer and 100 mM potassium acetate solution, and 18.75 pmol of *EGFP* mRNA in RNase-free water was added to the ALS−AuNP complex solution to induce the hybridization between ALS on AuNPs and the leader sequence (5′UTR) of mRNA. And the mixture was heated at 90 °C for 30 s using a heat block and slowly cooled down in warm D.I. water from 70 °C to R.T. for 30 min. After that, unhybridized mRNA was separated by centrifugation at 8000 rpm for 20 min. The hybridization efficiency was analyzed through the RiboGreen assay kit by measuring the FL intensity at an excitation wavelength of 480 nm and an emission wavelength of 530 nm with a microplate multimode reader.

Third, mRNA-ALS-citAuNP or mRNA-ALS-ggAuNP was encapsulated into LNP to improve the cellular uptake. In this step, prepared mRNA−ALS−AuNPs were dispersed in 11.06 μL of RNase-free water and 12.7 μL of 100 mM sodium acetate solution, and then this solution was manually mixed with 4.24 μL of ethanolic LNP (molar ratio: 49.28:10.75:0.75:16.06 = Ionizable lipid: Phospholipid: PEG lipid: protopanaxadiol (PPD)) solution. After that, the mixture was vigorously vortexed for 1 min, incubated for 15 min at R.T., and then sonicated for 1 min to complete the reaction. An additional 70 μL of RNase-free water was added to achieve a total volume of 100 μL for further experiments. For the FR targeting mRNA delivery test, DMG 2000 PEG lipid was replaced with DSPE-PEG(2000)-folate in the LNP formulation.

Calculation of ALS Binding Efficiency Using Qubit. The binding efficiency of ALS on the AuNP with several concentrations of ALS from 10 to 30 pmol was estimated by using the Qubit assay kit and FL reader, applying eq 1.

$$\text{Binding Efficiency (\%)} = 1 - \left(\frac{\text{FL value from ALS in the supernatant after the binding reaction}}{\text{FL value at the applied ALS condition}} \right) \times 100 \quad (1)$$

Direct measurement of FL values from ALS on AuNPs was avoided due to potential interference from the plasmonic properties of AuNPs. The plasmonic energy transfer from AuNPs to FL dye in ALS could occur,[61,62] potentially leading to inaccurate FL measurements. Therefore, in this study, the unbound ALS was separated by centrifugation after the binding reaction under each concentration condition, and the FL value of the ALS in the supernatant was measured.

Calculation of mRNA Hybridization Efficiency Using the RiboGreen Assay. The hybridization efficiency of mRNA with ALS on the AuNP was evaluated using a RiboGreen assay kit and a microplate reader (eq 2, which follows a similar approach to the calculation of ALS binding efficiency).

$$\text{Hybridization Efficiency (\%)} = 1 - \left(\frac{\text{FL value from mRNA in the supernatant after the reaction}}{\text{FL value at the applied mRNA condition}} \right) \times 100 \quad (2)$$

mRNA Protection Test against RNase. To assess the stability of mRNA on the ALS−AuNPs or within the ALS-AuNP@LNP against RNase, naked *EGFP* mRNA, *EGFP* mRNA-ALS-citAuNP, or *EGFP* mRNA-ALS-citAuNP@LNP were mixed with 0.01 μg of RNase. After treatment with RNase, the sample was incubated at 37 °C for 1 h, and then Proteinase K was added to the mixture and incubated continuously for 10 min to inactivate the RNase. After that, samples were analyzed on agarose gel electrophoresis (1.5%, 0.5 × TBE buffer).

Cell Culture. Lung cancer cell lines (A549), cervical carcinoma cell lines (HeLa), and kidney cell lines (HEK293T) were grown in cell culture plates for the expression test. Each cell line was cultured in RPMI medium and DMEM mixed with 10% FBS and Penicillin−Streptomycin in a 37 °C incubator under 5% CO_2 conditions.

In Vitro Transcription for mRNA Production. *EGFP* mRNA and *mCherry* mRNA were synthesized via PCR using Pfu Polymerase under the following conditions: 95 °C for 2 min (1 cycle); 95 °C, 20 s—60 °C, 40 s—72 °C, 2 min 30 s (30 cycles); 72 °C (5 min). The amplified PCR product was

https://doi.org/10.1021/acsomega.5c02145
ACS Omega 2025, 10, 32998−33007

electrophoresed using a 1.5% agarose gel, purified using the Qiaquick Gel Extraction Kit, and used as a template for IVT. 1 μg of the PCR product was reacted overnight in an incubator at 37 °C by adding 100 mM ATP, 100 mM CTP, 100 mM GTP, 100 mM UTP, 40000 U/ml RNase inhibitor, 50000 U/ml T7 polymerase, 100 U/ml pyrophosphatase, clean cap reagent AG, and 10× transcription buffer. After the reaction, 2 μL of DNase I was added, and the DNA template was removed by reacting at 37 °C for 15 min. After the IVT reaction, the reaction solution was purified using the Monarch RNA Cleanup kit and finally eluted in 50 μL of RNase-free distilled water. The purified mRNA was quantified using NanoDrop, and the mRNA product was confirmed by electrophoresis on agarose gel (1.5%, 0.5× TBE).

Viability Test. A549 cells were initially seeded at approximately 5 × 10^4 cells per well in 24-well plates. And to evaluate the biocompatibility of the carriers, citAuNP or ggAuNP was incubated with the cells at various concentrations ranging from 0 to 5 μg/μL. Following 24 h of incubation at 37 °C with 5% CO_2, cell viability was assessed using a CCK assay according to the manufacturer's protocol. After adding the assay reagent and incubating for an additional 1 h, absorbance was measured at 450 nm using a microplate reader to determine relative cell viability.

mRNA Delivery and Expression Test. To evaluate the delivery and expression efficiency of mRNA, *EGFP* mRNA-ALS-citAuNP@LNP or *EGFP* mRNA-ALS-ggAuNP@LNP, prepared under the above formulation condition, was incubated with A549, HeLa, and HEK293 cells seeded at 5 × 10^4 cells per well in 24-well plates. After 24 h of treatment, EGFP expression in the transfected cells was examined using a FL optical microscope. For the targeted delivery test, the same amount of *EGFP* mRNA-ALS-AuNP@LNP or *EGFP* mRNA-ALS-AuNP@folate-LNP was incubated with HeLa cells and A549 cells in 24-well plates, and after 24 h of incubation, EGFP expression in each cell line was observed via a FL optical microscope. For codelivery and expression of *EGFP*/*mCherry* mRNA, A549 cells were treated and observed 24 h post-treatment using a fluorescence microscope. The cells were then harvested, resuspended in PBS containing 1% FBS, and analyzed via flow cytometry to evaluate the expression efficiency.

Statistical Analysis. Statistical analysis was performed using one-way analysis of variance (ANOVA) with Tukey's test (OriginPro software, version 8.5), and statistically significant differences were defined as $*p < 0.05$ and $**p < 0.01$.

■ ASSOCIATED CONTENT

Supporting Information

The Supporting Information is available free of charge at https://pubs.acs.org/doi/10.1021/acsomega.5c02145.

FT-IR spectra of AuNPs, gel electrophoresis results for monitoring of surface modification of AuNPs with ALS and mRNA, binding ratio of ALS with citAuNP, nanoparticle tracking analysis (NTA) result, gel electrophoresis results for mRNA stability against RNase, cell viability test for biocompatibility, results of confocal microscopy analysis, observation of EGFP expression depending on the ALS length or weight ratio or targeting effect, and flow cytometry profile depending on the *EGFP* mRNA/*mCherry* mRNA ratio (PDF)

■ AUTHOR INFORMATION

Corresponding Authors

Jaewook Lee − *Genomictree Inc, Daejeon 34027, Republic of Korea;* orcid.org/0000-0001-7142-1724; Email: jwlee@genomictree.com

Sungwhan An − *Genomictree Inc, Daejeon 34027, Republic of Korea*; Email: sungwhan@genomictree.com

Authors

Dajeong Hwang − *Genomictree Inc, Daejeon 34027, Republic of Korea*

Sin A Park − *Genomictree Inc, Daejeon 34027, Republic of Korea*

Jae Hoon Kim − *Genomictree Inc, Daejeon 34027, Republic of Korea*

Seung-Yeul Lee − *Genomictree Inc, Daejeon 34027, Republic of Korea*

Jaebeom Lee − *Department of Chemistry and Department of Chemical Engineering and Applied Chemistry, Chungnam National University, Daejeon 34134, Republic of Korea;* orcid.org/0000-0002-8414-7290

Han Sang Kim − *Yonsei Cancer Center, Division of Medical Oncology, Department of Internal Medicine, Yonsei University College of Medicine, Seoul 03722, Republic of Korea; Department of Internal Medicine, Graduate School of Medical Science, Brain Korea 21 Project, Yonsei University College of Medicine, Seoul 03722, Republic of Korea*

Kyung-A Kim − *Department of Internal Medicine, Graduate School of Medical Science, Brain Korea 21 Project, Yonsei University College of Medicine, Seoul 03722, Republic of Korea*

Seung-Hoon Lee − *Department of Biotechnology, Yong-In University, Yongin 17092 Gyeonggi-do, Republic of Korea*

Tae Jeong Oh − *Genomictree Inc, Daejeon 34027, Republic of Korea*

Complete contact information is available at: https://pubs.acs.org/10.1021/acsomega.5c02145

Author Contributions

#D.H. and S.A.P. are equally contributing authors. D. Hwang: methodology, investigation, formal analysis, writing—original draft. S. A Park: methodology, investigation, formal analysis, writing—original draft. J. H. Kim: investigation, formal analysis. S.-Y. Lee: investigation, formal analysis. J. Lee: investigation, resource, writing—review and editing. H. S. Kim: resource, investigation, resource, writing—review and editing. K.-A Kim: investigation, writing—review and editing. S.-H. Lee: investigation, resource, writing—review and editing. T. J. Oh: project administration, writing—review and editing. J. Lee: conception, methodology, investigation, formal analysis, visualization, writing—original draft, writing—review and editing. and S. An: supervision, project administration, conception, writing—original draft, writing—review and editing.

Notes

The authors declare no competing financial interest.

■ ACKNOWLEDGMENTS

We thank the staff members at Genomictree, Inc., for technical support.

REFERENCES

(1) Liu, C.; Shi, Q.; Huang, X.; Koo, S.; Kong, N.; Tao, W. mRNA-based cancer therapeutics. *Nat. Rev. Cancer* **2023**, *23* (8), 526−543.
(2) Jahanafrooz, Z.; Baradaran, B.; Mosafer, J.; Hashemzaei, M.; Rezaei, T.; Mokhtarzadeh, A.; Hamblin, M. R. Comparison of DNA and mRNA vaccines against cancer. *Drug discovery today* **2020**, *25* (3), 552−560.
(3) Wadhwa, A.; Aljabbari, A.; Lokras, A.; Foged, C.; Thakur, A. Opportunities and challenges in the delivery of mRNA-based vaccines. *Pharmaceutics* **2020**, *12* (2), 102.
(4) Sahin, U.; Karikó, K.; Türeci, Ö. mRNA-based therapeutics-developing a new class of drugs. *Nat. Rev. Drug Discovery* **2014**, *13* (10), 759−780.
(5) Van Lint, S.; Goyvaerts, C.; Maenhout, S.; Goethals, L.; Disy, A.; Benteyn, D.; Pen, J.; Bonehill, A.; Heirman, C.; Breckpot, K.; et al. Preclinical evaluation of TriMix and antigen mRNA-based antitumor therapy. *Cancer Res* **2012**, *72* (7), 1661−1671.
(6) Qureischi, M.; Mohr, J.; Arellano-Viera, E.; Knudsen, S. E.; Vohidov, F.; Garitano-Trojaola, A. mRNA-based therapies: Preclinical and clinical applications. *Int Rev Cell Mol Biol* **2022**, *372*, 1−54.
(7) Zhou, L.-Y.; Qin, Z.; Zhu, Y.-H.; He, Z.-Y.; Xu, T. Current RNA-based therapeutics in clinical trials. *Curr. Gene Ther.* **2019**, *19* (3), 172−196.
(8) Lei, S.; Zhang, X.; Li, J.; Gao, Y.; Wu, J.; Duan, X.; Men, K. Current progress in messenger RNA-based gene therapy. *J. Biomed. Nanotechnol.* **2020**, *16* (7), 1018−1044.
(9) Zhang, W.; Jiang, Y.; He, Y.; Boucetta, H.; Wu, J.; Chen, Z.; He, W. Lipid carriers for mRNA delivery. *Acta Pharm. Sin. B* **2023**, *13* (10), 4105−4126.
(10) Loh, X. J.; Lee, T.-C.; Dou, Q.; Deen, G. R. Utilising inorganic nanocarriers for gene delivery. *Biomater. Sci* **2016**, *4* (1), 70−86.
(11) Xu, Z. P.; Zeng, Q. H.; Lu, G. Q.; Yu, A. B. Inorganic nanoparticles as carriers for efficient cellular delivery. *Chem. Eng. Sci.* **2006**, *61* (3), 1027−1040.
(12) Yan, Y.; Xiong, H.; Zhang, X.; Cheng, Q.; Siegwart, D. J. Systemic mRNA delivery to the lungs by functional polyester-based carriers. *Biomacromolecules* **2017**, *18* (12), 4307−4315.
(13) Lu, Y.; Huang, W.; Li, M.; Zheng, A. Exosome-based carrier for RNA delivery: progress and challenges. *Pharmaceutics* **2023**, *15* (2), 598.
(14) Guan, S.; Rosenecker, J. Nanotechnologies in delivery of mRNA therapeutics using nonviral vector-based delivery systems. *Gene Ther* **2017**, *24* (3), 133−143.
(15) Yeom, J.-H.; Ryou, S.-M.; Won, M.; Park, M.; Bae, J.; Lee, K. Inhibition of xenograft tumor growth by gold nanoparticle-DNA oligonucleotide conjugates-assisted delivery of BAX mRNA. *PloS one* **2013**, *8* (9), No. e75369.
(16) Mbatha, L. S.; Maiyo, F.; Daniels, A.; Singh, M. Dendrimer-coated gold nanoparticles for efficient folate-targeted mRNA delivery in vitro. *Pharmaceutics* **2021**, *13* (6), 900.
(17) Kyriazi, M.-E.; Giust, D.; El-Sagheer, A. H.; Lackie, P. M.; Muskens, O. L.; Brown, T.; Kanaras, A. G. Multiplexed mRNA sensing and combinatorial-targeted drug delivery using DNA-gold nanoparticle dimers. *ACS Nano* **2018**, *12* (4), 3333−3340.
(18) Kus-Liśkiewicz, M.; Fickers, P.; Ben Tahar, I. Biocompatibility and cytotoxicity of gold nanoparticles: recent advances in methodologies and regulations. *Int. J. Mol. Sci* **2021**, *22* (20), 10952.
(19) Lim, Z.-Z. J.; Li, J.-E. J.; Ng, C.-T.; Yung, L.-Y. L.; Bay, B.-H. Gold nanoparticles in cancer therapy. *Acta Pharmacol. Sin.* **2011**, *32* (8), 983−990.
(20) Yang, C.; Bromma, K.; Di Ciano-Oliveira, C.; Zafarana, G.; van Prooijen, M.; Chithrani, D. B. Gold nanoparticle mediated combined cancer therapy. *Cancer Nanotechnol* **2018**, *9*, 4.
(21) Brockman, J. M.; Frutos, A. G.; Corn, R. M. A multistep chemical modification procedure to create DNA arrays on gold surfaces for the study of protein− DNA interactions with surface plasmon resonance imaging. *J. Am. Chem. Soc.* **1999**, *121* (35), 8044−8051.
(22) Smith, E. A.; Wanat, M. J.; Cheng, Y.; Barreira, S. V.; Frutos, A. G.; Corn, R. M. Formation, spectroscopic characterization, and application of sulfhydryl-terminated alkanethiol monolayers for the chemical attachment of DNA onto gold surfaces. *Langmuir* **2001**, *17* (8), 2502−2507.
(23) Zhou, J.; Ralston, J.; Sedev, R.; Beattie, D. A. Functionalized gold nanoparticles: synthesis, structure and colloid stability. *J. Colloid Interface Sci.* **2009**, *331* (2), 251−262.
(24) Ahmed, H. B. Recruitment of various biological macromolecules in fabrication of gold nanoparticles: overview for preparation and applications. *Int. J. Biol. Macromol.* **2019**, *140*, 265−277.
(25) Zhang, H.; Gao, Z.; Li, X.; Li, L.; Ye, S.; Tang, B. Multiple-mRNA-controlled and heat-driven drug release from gold nanocages in targeted chemo-photothermal therapy for tumors. *Chem. Sci.* **2021**, *12* (37), 12429−12436.
(26) Graczyk, A.; Pawlowska, R.; Chworos, A. Gold Nanoparticles as Carriers for Functional RNA Nanostructures. *Bioconjugate Chem.* **2021**, *32* (8), 1667−1674.
(27) Singh, P.; Mijakovic, I. Advances in gold nanoparticle technology as a tool for diagnostics and treatment of cancer. *Expert Rev. Mol. Diagn* **2021**, *21* (7), 627−630.
(28) Rosyidah, A. l.; Kerdtoob, S.; Yudhistyra, W. I.; Munfadlila, A. W. Gold nanoparticle-based drug nanocarriers as a targeted drug delivery system platform for cancer therapeutics: a systematic review. *Gold Bull* **2023**, *56* (3), 121−134.
(29) Luo, D.; Wang, X.; Burda, C.; Basilion, J. P. Recent Development of Gold Nanoparticles as Contrast Agents for Cancer Diagnosis. *Cancers* **2021**, *13* (8), 1825.
(30) Uddin, M. D. I.; Kilburn, T. C.; Yang, R.; McCollum, G. W.; Wright, D. W.; Penn, J. S. Targeted Imaging of VCAM-1 mRNA in a Mouse Model of Laser-Induced Choroidal Neovascularization Using Antisense Hairpin-DNA-Functionalized Gold-Nanoparticles. *Mol. Pharmaceutics* **2018**, *15* (12), 5514−5520.
(31) Han, G.; Martin, C. T.; Rotello, V. M. Stability of Gold Nanoparticle-Bound DNA toward Biological, Physical, and Chemical Agents. *Chem. Biol. Drug Des.* **2006**, *67* (1), 78−82.
(32) Ding, Y.; Jiang, Z.; Saha, K.; Kim, C. S.; Kim, S. T.; Landis, R. F.; Rotello, V. M. Gold Nanoparticles for Nucleic Acid Delivery. *Mol. Ther.* **2014**, *22* (6), 1075−1083.
(33) Son, S.; Kim, N.; You, D. G.; Yoon, H. Y.; Yhee, J. Y.; Kim, K.; Kwon, I. C.; Kim, S. H. Antitumor therapeutic application of self-assembled RNAi-AuNP nanoconstructs: Combination of VEGF-RNAi and photothermal ablation. *Theranostics* **2017**, *7* (1), 9−22.
(34) Jeon, M.; Kim, G.; Lee, W.; Baek, S.; Jung, H. N.; Im, H.-J. Development of theranostic dual-layered Au-liposome for effective tumor targeting and photothermal therapy. *J. Nanobiotechnol.* **2021**, *19* (1), 262.
(35) Grafals-Ruiz, N.; Rios-Vicil, C. I.; Lozada-Delgado, E. L.; Quiñones-Díaz, B. I.; Noriega-Rivera, R. A.; Martínez-Zayas, G.; Santana-Rivera, Y.; Santiago-Sánchez, G. S.; Valiyeva, F.; Vivas-Mejía, P. E. Brain Targeted Gold Liposomes Improve RNAi Delivery for Glioblastoma. *Int. J. Nanomedicine* **2020**, *15*, 2809−2828.
(36) Park, S. A.; Hwang, D.; Kim, J. H.; Lee, S.-Y.; Lee, J.; Kim, H. S.; Kim, K.-A.; Lim, B.; Lee, J.-E.; Jeon, Y. H.; et al. Formulation of lipid nanoparticles containing ginsenoside Rg2 and protopanaxadiol for highly efficient delivery of mRNA. *Biomater. Sci.* **2024**, *12* (24), 6299−6309.
(37) Pardi, N.; Hogan, M. J.; Weissman, D. Recent advances in mRNA vaccine technology. *Curr Opin Immunol* **2020**, *65*, 14−20.
(38) Reichmuth, A. M.; Oberli, M. A.; Jaklenec, A.; Langer, R.; Blankschtein, D. mRNA vaccine delivery using lipid nanoparticles. *Ther. Deliv* **2016**, *7* (5), 319−334.
(39) Zhang, N.-N.; Li, X.-F.; Deng, Y.-Q.; Zhao, H.; Huang, Y.-J.; Yang, G.; Huang, W.-J.; Gao, P.; Zhou, C.; Zhang, R.-R.; et al. A thermostable mRNA vaccine against COVID-19. *Cell* **2020**, *182* (5), 1271−1283.e16.
(40) Wang, H.-X.; Zuo, Z.-Q.; Du, J.-Z.; Wang, Y.-C.; Sun, R.; Cao, Z.-T.; Ye, X.-D.; Wang, J.-L.; Leong, K. W.; Wang, J. Surface charge

https://doi.org/10.1021/acsomega.5c02145
ACS Omega 2025, 10, 32998−33007

critically affects tumor penetration and therapeutic efficacy of cancer nanomedicines. *Nano Today* **2016**, *11* (2), 133−144.
(41) Mintzer, M. A.; Simanek, E. E. Nonviral vectors for gene delivery. *Chem. Rev.* **2009**, *109* (2), 259−302.
(42) Aoshima, Y.; Hokama, R.; Sou, K.; Sarker, S. R.; Iida, K.; Nakamura, H.; Inoue, T.; Takeoka, S. Cationic amino acid based lipids as effective nonviral gene delivery vectors for primary cultured neurons. *ACS Chem. Neurosci* **2013**, *4* (12), 1514−1519.
(43) Liu, J.; Jiang, X.; Ashley, C.; Brinker, C. J. Electrostatically mediated liposome fusion and lipid exchange with a nanoparticle-supported bilayer for control of surface charge, drug containment, and delivery. *J. Am. Chem. Soc.* **2009**, *131* (22), 7567−7569.
(44) Dathe, M.; Schümann, M.; Wieprecht, T.; Winkler, A.; Beyermann, M.; Krause, E.; Matsuzaki, K.; Murase, O.; Bienert, M. Peptide helicity and membrane surface charge modulate the balance of electrostatic and hydrophobic interactions with lipid bilayers and biological membranes. *Biochemistry* **1996**, *35* (38), 12612−12622.
(45) He, C.; Hu, Y.; Yin, L.; Tang, C.; Yin, C. Effects of particle size and surface charge on cellular uptake and biodistribution of polymeric nanoparticles. *Biomaterials* **2010**, *31* (13), 3657−3666.
(46) Yue, Z.-G.; Wei, W.; Lv, P.-P.; Yue, H.; Wang, L.-Y.; Su, Z.-G.; Ma, G.-H. Surface charge affects cellular uptake and intracellular trafficking of chitosan-based nanoparticles. *Biomacromolecules* **2011**, *12* (7), 2440−2446.
(47) Yu, B.; Zhang, Y.; Zheng, W.; Fan, C.; Chen, T. Positive surface charge enhances selective cellular uptake and anticancer efficacy of selenium nanoparticles. *Inorg. Chem* **2012**, *51* (16), 8956−8963.
(48) Kettler, K.; Veltman, K.; van De Meent, D.; van Wezel, A.; Hendriks, A. J. Cellular uptake of nanoparticles as determined by particle properties, experimental conditions, and cell type. *Environ. Toxicol. Chem* **2013**, *33* (3), 481−492.
(49) Andrée, L.; Oude Egberink, R.; Dodemont, J.; Hassani Besheli, N.; Yang, F.; Brock, R.; Leeuwenburgh, S. C. Gelatin nanoparticles for complexation and enhanced cellular delivery of mRNA. *Nanomaterials* **2022**, *12* (19), 3423.
(50) Kim, J.; Copeland, C. E.; Kwon, Y.-C. Harnessing nanoreactors: gelatin nanogels for human therapeutic protein delivery. *Mater Adv* **2024**, *5*, 5527−5542.
(51) Saber, M. M. Strategies for surface modification of gelatin-based nanoparticles. *Colloids Surf., B* **2019**, *183*, 110407.
(52) Yasmin, R.; Shah, M.; Khan, S. A.; Ali, R. Gelatin nanoparticles: A potential candidate for medical applications. *Nanotechnol. Rev.* **2017**, *6* (2), 191−207.
(53) Rennick, J. J.; Johnston, A. P.; Parton, R. G. Key principles and methods for studying the endocytosis of biological and nanoparticle therapeutics. *Nat. Nanotechnol* **2021**, *16* (3), 266−276.
(54) Sousa de Almeida, M.; Susnik, E.; Drasler, B.; Taladriz-Blanco, P.; Petri-Fink, A.; Rothen-Rutishauser, B. Understanding nanoparticle endocytosis to improve targeting strategies in nanomedicine. *Chem. Soc. Rev.* **2021**, *50* (9), 5397−5434.
(55) Zhang, S.; Gao, H.; Bao, G. Physical principles of nanoparticle cellular endocytosis. *ACS Nano* **2015**, *9* (9), 8655−8671.
(56) Fröhlich, E. The role of surface charge in cellular uptake and cytotoxicity of medical nanoparticles. *Int. J. Nanomed* **2012**, 5577−5591.
(57) Gustafson, H. H.; Holt-Casper, D.; Grainger, D. W.; Ghandehari, H. Nanoparticle uptake: the phagocyte problem. *Nano today* **2015**, *10* (4), 487−510.
(58) Vácha, R.; Martinez-Veracoechea, F. J.; Frenkel, D. Receptor-mediated endocytosis of nanoparticles of various shapes. *Nano Lett.* **2011**, *11* (12), 5391−5395.
(59) Xu, S.; Olenyuk, B. Z.; Okamoto, C. T.; Hamm-Alvarez, S. F. Targeting receptor-mediated endocytotic pathways with nanoparticles: rationale and advances. *Adv. Drug Deliv. Rev* **2013**, *65* (1), 121−138.
(60) Zhang, X.; Servos, M. R.; Liu, J. Instantaneous and Quantitative Functionalization of Gold Nanoparticles with Thiolated DNA Using a pH-Assisted and Surfactant-Free Route. *J. Am. Chem. Soc.* **2012**, *134* (17), 7266−7269.
(61) Lee, J.; Ahmed, S. R.; Oh, S.; Kim, J.; Suzuki, T.; Parmar, K.; Park, S. S.; Lee, J.; Park, E. Y. A plasmon-assisted fluoro-immunoassay using gold nanoparticle-decorated carbon nanotubes for monitoring the influenza virus. *Biosens. Bioelectron.* **2015**, *64*, 311−317.
(62) Lee, J.; Kim, J.; Ahmed, S. R.; Zhou, H.; Kim, J.-M.; Lee, J. Plasmon-Induced Photoluminescence Immunoassay for Tuberculosis Monitoring Using Gold-Nanoparticle-Decorated Graphene. *ACS Appl. Mater. Interfaces* **2014**, *6* (23), 21380−21388.

https://doi.org/10.1021/acsomega.5c02145
ACS Omega 2025, 10, 32998−33007